

Shear cutting of press hardened steel: influence of punch chamfer on process forces, tool stresses and sheared edge qualities

Katrin Nothhaft · Jounghsik Suh · Matthias Golle ·
Ingrid Picas · Daniel Casellas · Wolfram Volk

Received: 20 April 2012 / Accepted: 9 July 2012 / Published online: 19 July 2012
© German Academic Society for Production Engineering (WGP) 2012

Abstract In order to cope with the difficulties of shearing operations of press hardened steels, this work attempted to optimize these processes. Herefore, it is necessary to reduce the press forces and stresses in tools, while still obtaining adequate sheared edge quality levels. To reach this goal, different punch chamfer angles (0° , 2° , 7° and 20°) and relative cutting clearances (5, 10 and 15 % of the sheet thickness) were tested in a cutting tool, which was adapted in a way that different active elements could be mounted. The tool was equipped with a measurement system, which allowed the determination of the process forces in three dimensions at each punch stroke. Basis was an AlSi coated 22MnB5 sheet with a thickness of 1.5 mm. In addition a finite element model was developed to predict the stress distribution in tools and the sheared edge qualities. According to the experimental results the application of a 20° chamfer angle succeeded to reduce the forces and

stresses of tools, but the sheared parts had a poor quality. In contrast, the 7° chamfer angle gave lowest tool stresses and sufficient part qualities, but the forces were very high. The simulation results agreed with the experimental data, except for the prediction of the rollover zone. These deviations were attributed among others to the presence of the AlSi coating, which was not considered.

Keywords Shear cutting · Press hardened steel · Force measurement · FEA

1 Introduction

The development of integrated lightweight designs and the use of smart materials and manufacturing processes offer the automotive industry a substantial opportunity to successfully upgrade the current vehicle standards according to the increasing demands on safety and sustainability. However, to implement lightweight designs in cars, criteria such as functionality, production volume and costs must first be harmonized. The accomplishment of this aim will depend on the right choice of materials, the performance and efficiency of the manufacturing processes, which allow to produce vehicle parts from them.

Steel and aluminum are already part of many lightweight designs, and fiber-reinforced plastics will also soon be used for structural parts [1]. Moreover, press hardening technologies are steadily broadening their application in the field of steel components, since they offer considerable potential for minimizing component weight by reducing the sheet thickness and producing components with tailored distributions of microstructural and mechanical properties [2]. However, one of the main discomforts of using such press hardened steels (PHS) lies in post forming

K. Nothhaft (✉) · J. Suh · W. Volk
Institute of Metal Forming and Casting,
Technical University Munich, Munich, Germany
e-mail: kn@utg.de

J. Suh
e-mail: js@utg.de

W. Volk
e-mail: wv@utg.de

M. Golle
Institute of Stamping, Pforzheim University,
Pforzheim, Germany
e-mail: mg@utg.de

I. Picas · D. Casellas
CTM Centre Tecnològic, Manresa, Spain
e-mail: Ingrid.picas@ctm.com.es

D. Casellas
e-mail: Daniel.casellas@ctm.com.es

processes, namely trimming or punching, which give the components their final geometry. Industrial shearing processes of PHS lead to symptomatic reduction of tool life cycles due to the high required forces which directly influence tool wear and numerous cutting shocks that also negatively affect the press functionality [3]. High stresses inside the tool, which can lead to early tool failure due to chipping or fracture, are the consequence. The application of warm and hot shearing operations is currently being studied while the application of novel laser-assisted cutting techniques is gaining acceptance among press hardening users due to the latest improvements regarding efficiency and productivity [4].

Considering mass production, shearing in a press is still more attractive than other cutting techniques due to its high productivity rates and low cost. Thus, in this work it is desired to optimize shearing operations for PHS by reducing process forces and tool stresses, but still achieving adequate quality levels. Mackensen et al. [3] has shown that standard shear cutting parameters, such as clearances and cutting angles, have a significant influence on the forces in a blanking process of advanced high-strength steels (AHSS) and the shear angle significantly reduces the cutting force. Picas et al. [5] in turn, has investigated the punching process of DP1000 steel and has concluded that nominal clearances must be comprised between the 10 and 15 % of the sheet thickness in order to prevent burr formation and increase tool life. The presence of burrs and other irregularities originated by shearing processes strongly influence the mechanical behavior of PHS components, e.g. their sensitivity to fatigue is very high [6], therefore it is convenient to optimize press shearing processes to reduce cutting forces, increase tool life and reduce irregularities of sheet fractured edges.

With the aim of predicting the resulting sheet edge shapes, the required forces and the stresses generated in tools during shearing processes, numerical analyses are typically performed by many authors. However, one major difficulty of these analyses is the description of the ductile fracture initiation, and many works have shown that selecting fracture criteria might be harsh in the sense that they fail at giving consistent results also for operating conditions outside the calibration range [7]. However, So et al. [8] using a Brozzo criterion with a critical damage value C of 0.95, predicted the shape of the cutting edge of a PHS in a blanking operation and they obtained a good approximation with respect to the experimental results.

The objective of this work was to describe well the phases of a shearing process of PHS, establishing the elastic and plastic pre-bending steps and the registered forces and stress distributions with regard to different clearances and chamfer angles. To reach this goal, an experimental set-up consisting in a tool design that allows

to measure process forces in three dimensions came to use, so not only cutting but also shearing forces were obtained. A finite element (FE) model was developed and the numerical analysis of the process permitted to determine the stress distribution generated in tools during one stroke and to predict the shape of the sheared edges. Simulation results were validated by the experimental tests, therefore proper changes could be made in the model in order to guarantee accurate results.

2 Experimental setup

The shear cutting tool, which had been developed at the utg and was introduced in Mackensen et al. [3] is used. It is equipped with a measurement system, which allows the determination of process forces in three dimensions and their correlation to the punch stroke.

Figure 1 shows the tool. It consists of three main parts: upper tool, blankholder and lower tool. Within the lower tool, four guide pillars are attached to the base plate and a supporting guiding plate is integrated to accommodate the shearing forces in x -direction. Furthermore the die is attached to the die adapter, which can be moved on the base plate in horizontal direction. The blankholder inlet is attached to the blankholder plate. Via two gas pressure springs, located in the upper tool, it applies the necessary forces to clamp the sheet between die and blankholder inlet during the cutting process. The punch, which is located in the upper tool as well, is attached to the punch block. Here four piezo-electric load cells are integrated and connected in parallel. As the force measurement is carried out in main force flow (direct force measurement), the load cells have to be preloaded. Thus shearing forces can be transferred by static friction between base and cover plates to the surface of the sensor. A preloading of 160 kN per sensor additionally provides sufficient stiffness within the punch block, which is needed to guarantee a constant cutting clearance during the cutting process. To detect the movement of the punch an inductive displacement transducer is attached to the lower tool and measures the distance to the top plate during the cutting process. This measuring system is able to detect the components of the resultant force vector and correlate them to the punch position.

Furthermore different active elements can be mounted on the tool, which allows testing different punch geometries regarding their chamfer angles as shown in Fig. 2. Besides the punch geometry, also the cutting clearance is adjustable.

The relative cutting clearances 5, 10 and 15 % of sheet thickness and the chamfer angles 0° , 2° , 7° and 20° at the punch were examined, while the die was always kept non chamfered. To verify the repeatability five strokes were

Fig. 1 Design of shear cutting tool

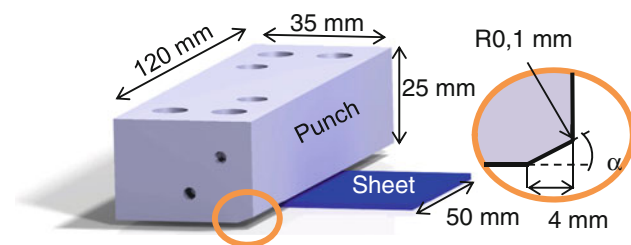
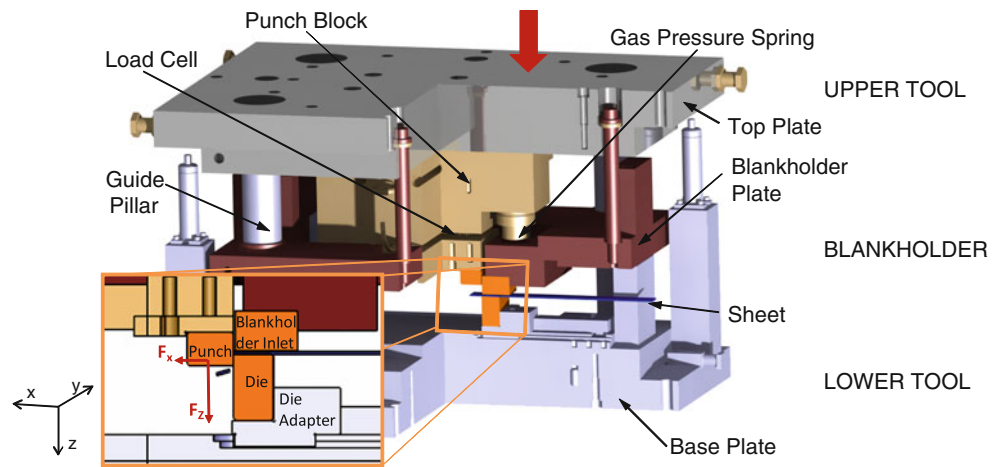


Fig. 2 Punch geometry; chamfer angle $\alpha = 0^\circ, 2^\circ, 7^\circ,$ and 20°

accomplished for each configuration. The used sheet material was Aluminum Silicon (AlSi)-coated, press-hardened 22MnB5 with a thickness of 1.5 mm and was provided by Gestamp HardTech. Its characteristic properties are as follows: $Re = 1,100$ MPa; $Rm = 1,500$ MPa; $A_{80} = 5\%$. The tests were carried out on a single-action hydraulic press with a maximum capacity of 3,200 kN. The tool was mounted in the press by connecting the top plate to the press slide and the base plate to the press table via mounting devices.

Part quality in respect to cutting clearance and chamfer angle was examined in addition to process forces. Therefore the cut parts were analyzed with a profile measurement device of Mahr Company (MarWin XC 20, PCV). With a scanning accuracy of $1\ \mu\text{m}$ a thin needle scratches along the sheared edge and thus detects the size of the parameters rollover, clean-shear, fracture and burr. Out of each test series all five parts were analyzed with three profile measurements on each part.

3 Material model and finite element modeling

3.1 Plasticity modeling and characterization

The researched PHS sheets were provided by Gestamp HardTech. For the simplified material characterization it was assumed that these press hardened sheets exhibit

insignificant anisotropy in plasticity. That is, the material behavior is isotropic and hence von Mises isotropic yield criterion was applied in this paper. Furthermore, the associated flow rule and isotropic hardening were used for the yield function. Two empirical models Ludwik, Eq. (1) and Hockett-Sherby, Eq. (2) were used to describe the material hardening at a high strain.

$$\bar{\sigma} = \sigma_0 + A\bar{\epsilon}^n \tag{1}$$

$$\bar{\sigma} = \sigma_{\text{sat}} - (\sigma_{\text{sat}} - \sigma_0) \cdot \exp(-k\bar{\epsilon}^m) \tag{2}$$

where $\bar{\sigma}$ and $\bar{\epsilon}$ are equivalent stress and strain defined by the yield condition, while A , n , σ_0 , σ_{sat} , k and m are material parameters to be calibrated. These hardening parameters were determined by fitting the averaged stress-strain curve obtained from uniaxial tensile tests along the rolling direction. For the present 22MnB5 sheet the parameters are: $A = 1,628.8$, $n = 0.362$, $\sigma_0 = 1,170.2$, $\sigma_{\text{sat}} = 1,645.7$, $k = 72.602$ and $m = 0.898$. Based on this, it was possible to achieve a best fit to the experimental tensile test data using a linear combination of two models with the linear combination factor α of 0.11 as follows:

$$\bar{\sigma} = \alpha \cdot \bar{\sigma}_{\text{Ludwik}} + (1 - \alpha) \cdot \bar{\sigma}_{\text{Hockett-Sherby}} \tag{3}$$

As the determined flow curve was achieved only from the tensile test data, the simulation results were verified by the experimental data of the presented shear cutting tests. Fig. 3 shows the material hardening curves with the calibrated parameters.

3.2 Phenomenological fracture criterion

The damage evolution of phenomenological fracture criteria is represented by the definition of the overall damage variable as follows:

$$D = \int_0^{\bar{\epsilon}_f} \frac{d\bar{\epsilon}}{\bar{\epsilon}_f(\eta, \theta)} \tag{4}$$

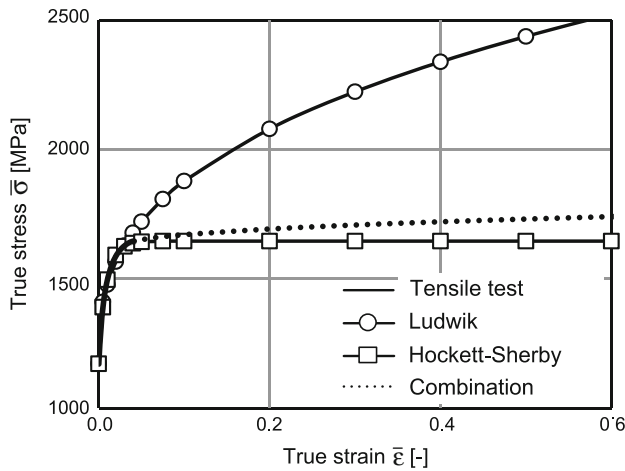


Fig. 3 Plastic hardening curves of press hardened 22MnB5

where $\bar{\epsilon}$ is the equivalent plastic strain, η is the stress triaxiality, $\eta = \sigma_m / \bar{\sigma}$, σ_m is the mean stress, $\bar{\sigma}$ is the equivalent stress and $\bar{\theta}$ is the normalized Lode angle, which is defined as

$$\bar{\theta} = 1 - \frac{6\theta}{\pi} \tag{5}$$

Since the range of Lode angle is $0 \leq \theta \leq \pi/3$, the range of $\bar{\theta}$ is $-1 \leq \bar{\theta} \leq 1$. The fracture occurs when the damage indicator $D = 1$ on the assumption that damage is characterized by the progressive degradation of the material stiffness and thus leads to failure [9].

According to the most recent study [10], the fracture locus is a monotonic function of the stress triaxiality parameter η , and an asymmetric function of the Lode angle parameter $\bar{\theta}$. This equation represents the locus of all stress states under which fracture is achieved along the proportional loading path. This function could be either found by fitting a certain number of experimental points or by making use of a phenomenological model such as the Modified Mohr–Coulomb (MMC) fracture criterion [10]. According to this model, if a von Mises yield function is used, the function $\bar{\epsilon}_f(\eta, \bar{\theta})$ is uniquely defined by the following form:

$$\bar{\epsilon}_f(\eta, \bar{\theta}) = \left\{ \frac{A}{C_2} \left[\sqrt{\frac{1+C_1^2}{3}} \cos\left(\frac{\bar{\theta}\pi}{6}\right) + C_1 \left(\eta + \frac{1}{3} \sin\left(\frac{\bar{\theta}\pi}{6}\right) \right) \right] \right\}^{-1/n} \tag{6}$$

where A and n are the strength coefficient and the exponent of the hardening rule, respectively. The fracture parameter C_1 is often referred to as a friction coefficient and C_2 is shear resistance [11]. The procedure for calibrating the fracture parameters is described in detail in [12]. For the

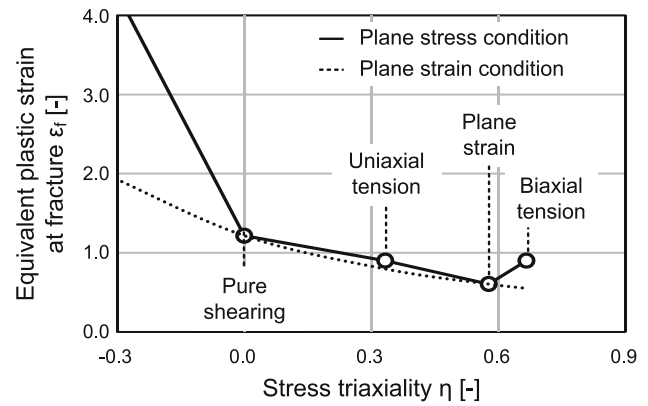


Fig. 4 2D MMC fracture loci under plane stress and plane strain conditions

present 22MnB5, the plasticity and fracture parameters are: $A = 1,628.8$, $n = 0.362$, $C_1 = 0.3$ and $C_2 = 1,053.9$ and the 2D MMC fracture locus is displayed in Fig. 4.

This calculated fracture model is used in shear cutting simulations.

3.3 Finite element modeling

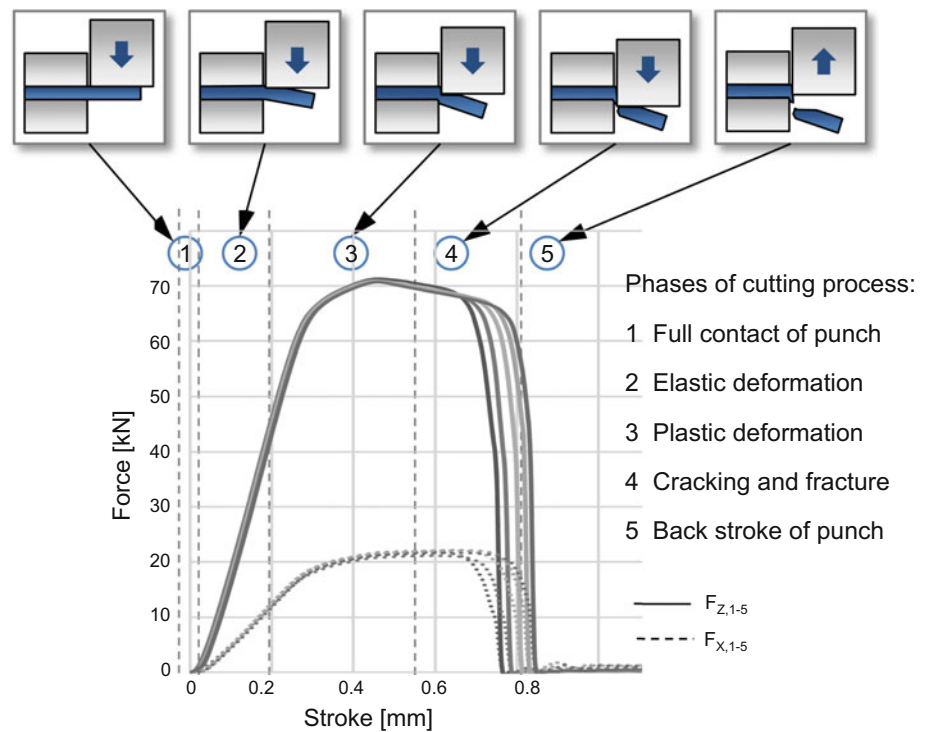
All the finite element simulations of the present cutting processes are performed with ABAQUS/Explicit v6.10. Having a sheet width that is far larger than the sheet thickness, the shear cutting process is modeled two-dimensionally under the plain strain condition. The finite element model consists of blankholder, punch, die and elasto-plastic sheet. To evaluate the stress distribution of the punch and die during the cutting process, the punch and die are modeled as elastically deformable bodies and the blankholder as rigid body in ABAQUS. The sheet is modeled by 17000 four-node plain-strain solid elements with reduced integration technique (CPE4R). The crack initiation and propagation is simulated using the element deletion technique. To run the simulations more efficiently without distorting results, an acceptable mass scaling (100 times) is employed. A constant related blankholder force of 400 N/mm clamps the sheet during the cutting process. All existing contacts are modeled with a standard friction coefficient of 0.1.

4 Results and discussion

4.1 Experimental results

Figure 5 shows the process forces curves for a non chamfered punch at 5 % cutting clearance. The curves match very well regarding the maximum forces and therefore demonstrate good repeatability of the cutting tests. The

Fig. 5 Cutting forces F_Z and shearing forces F_X during shear cutting process of PHS in experimental testing, sheet thickness: 1.5 mm, sheet width: 50 mm, relative cutting clearance: 5 %, non-chamfered punch, five test series



point of fracture varies within 0.04 mm. Furthermore it depicts the five stages of the cutting process. In stage one, represented by the positive curvature in the origin, the punch touches the sheet. In stage two further penetration of the punch leads to elastic deformations and thus to a linear acceleration of the curve. Here a bending moment based on the cutting and the shearing forces is induced around the cutting edge of the die and bends the sheet. Thus, the punch only contacts the sheet within a small rectangular area, as the remaining sheet lifts off. When the linear curve starts to curve negatively the third stage begins. At this point the yield strength of the sheet material is reached and it deforms plastically. The material is being work-hardened while the cross section area reduces. After the maximum cutting force is reached, the reduction of the section area predominates, which leads to a decrease of the cutting force. The maximum measured cutting force is 71.1 kN. A theoretical calculation of the cutting force can be done with Eq. (7):

$$F_{\max} = c \cdot s \cdot l \cdot \sigma_m \tag{7}$$

Here s is the sheet thickness, l the sheet width and c the shearing constant, which depends on the sheet material. In general it varies between 0.6 for material showing high yield strength and 0.9 for materials with low yield strength. Using 0.6 the theoretical value adds up to 69.8 kN, showing a deviation of 1.9 % to the experimental value.

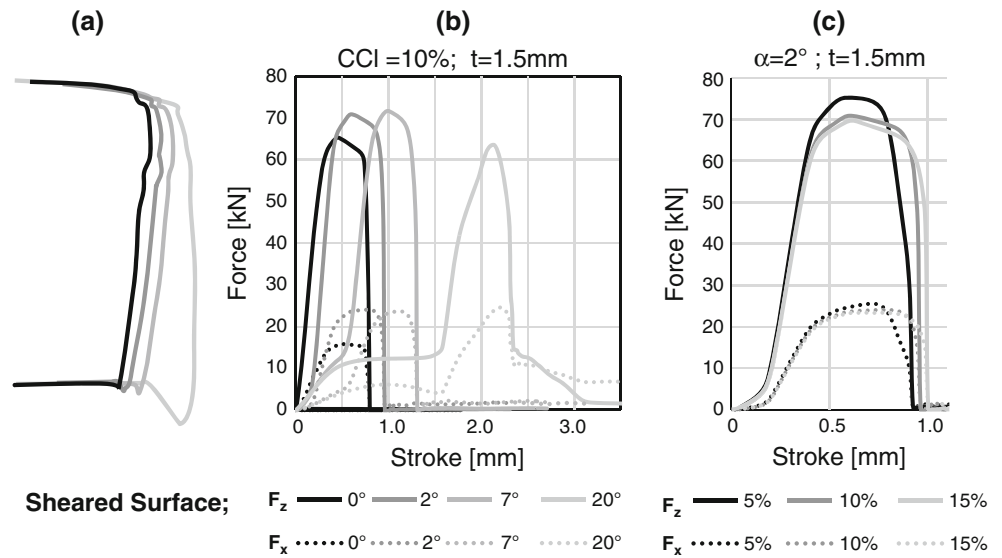
The appearance of small cracks in the sheet indicates that its fracture strength is reached. The cracks eventually lead to complete fracture, which is represented in the steep decline

of the curves in stage four. The fracture releases the elastic energy of the press, which usually manifests in oscillations of the curve. In this press, however cutting impact dampers were used, which compensate the oscillations. In stage five, which was not an object of investigation, the punch moves back up. The shearing forces show similar curves as the cutting forces with a much lower and less distinct maximum.

Figure 6b shows the process forces curves in respect of the chamfer angles. When chamfered punches are used the curves differ in discontinuance during their elastic acceleration. This is due to the plastic prebending through the chamfer. When the punch touches the material, a short period of elastic deformation is followed by plastic bend forming, which is dependent on the size of the chamfer angle. After the end of the chamfer is reached the cutting edge hits the material and starts the actual cutting process and the curves continue as shown in Fig. 5. For 2° and 7° angle the maximum forces are higher than for 0°. Only for 20° a reduction of the maximum force is reached. This is due to the strong prebending, which initiates small cracks before the cutting edge hits the sheet. Maximum shearing forces are higher for all chamfered punches.

In Fig. 6c the dependency of process forces on cutting clearance is shown on the example of a non chamfered punch. It can be seen that larger cutting clearances lead to lower maximum forces and later fracture. A larger cutting clearance generates larger bending due to the increased lever arm, which results in the described later fracture of the material. Further results regarding the part quality are

Fig. 6 Experimental results: Shearing Surface as a function of different chamfer angles (a), cutting and shearing forces as a function of different chamfer angles (b) and different cutting clearances (c)



shown in Figs. 6a and 7. As the sheet material is very brittle and its tensile strength is very high it shows comparable small values for rollover and clean-shear, but high percentage of fracture. Figure 6a shows the shearing surfaces for different chamfer angles. Rollover increases with an increasing chamfer angle due to prebending. The remaining surface parameters are very similar for 0°, 2° and 7° fracture angle. A different surface occurs only for 20° fracture angle. It consists of an inhomogeneous variation of clean-shear and fracture and a very large burr. With an increase of the cutting clearance as shown in Fig. 7 the sheared surfaces do not show significant differences. There is a small increase of rollover and decrease of the fracture angle β for an increased cutting clearance.

4.2 Validation of simulation model

To validate the simulation model sheared edge qualities and maximum forces from experimental testing were compared to simulation results. Figure 7 shows the sheared edge qualities for different cutting clearances. The goal was to establish the fracture criteria in a way that fracture starts at the same punch position as in experimental testing. Therefore the amount of rollover and clean-shear should match. A matching of clean-shear could be achieved well, regarding the rollover, however, large deviations occurred. A possible explanation for these deviations can be the AISi coating, which was not considered in the simulation. The reason is, that effects resulting from the inhomogeneity of

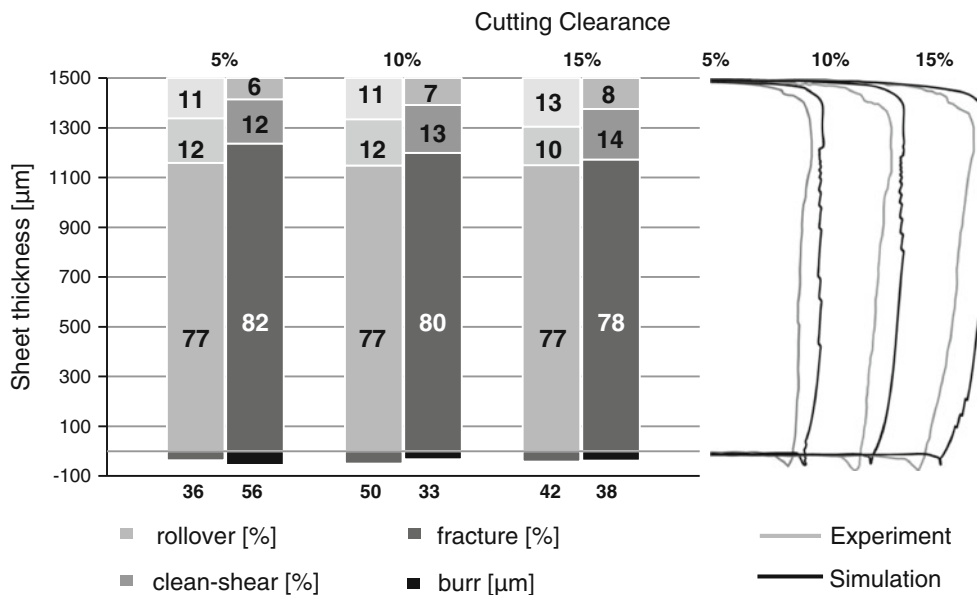


Fig. 7 Sheared edge quality, simulation versus experimental testing

the coating, lead to gradients in the third direction and therefore need a 3D model. Furthermore there are not enough material properties and mechanisms available for the realization of the coating in FE-simulation. In the experiments the coating chips of near the cutting edge. This is shown in the right side of Fig. 7 by the small step at the beginning of the sheared edge, which increases the size of the rollover zone. The differences in the area of fracture have only numerical reasons and no physical meaning.

Regarding the cutting forces, which are summarized in Fig. 9, a maximum deviation of 9 % occurs for 20° chamfer angle in combination with 5 % relative cutting clearance. The shearing forces show higher deviations, which can be again caused by the AlSi coating that supplies a rough surface with high friction values. This was proven by results from experiments with non-coated 22MnB5, which show reduced process forces. For 5 % relative cutting clearance the cutting forces were reduced by 2.7 % whereas the shearing forces were reduced by 16.5 % to 18.2 kN, which shows good correspondence with the simulation results.

Except for the coated layer the simulation results resemble the experimental results well enough to use the FE-model for the analysis of stress distribution within punch and die of the cutting tool.

4.3 Simulation results

A FE-Simulation was carried out to determine stress distributions within the active elements during the shear cutting process. The focus was set on the punch, as it commonly fails first. The following figure shows the von Mises stress distribution in the punch and the maximum von Mises stresses along the punch stroke. The absolute maximum of 2,100 MPa occurs at the change from elastic to plastic deformation of the material, which differs from the punch position that shows maximum forces. After the maximum is reached the stresses gradually decrease until the fracture is initiated and forces and stresses promptly decline to zero. Locally the maximum stresses occur in the area of the cutting radius, where they move along a bent line from I to VI as shown in Fig. 8.

A summary of all maximum von Mises stresses as well as all maximum process forces from simulation and experiment are shown in Fig. 9. The stresses behave contrary to the maximum forces. Hence an increasing cutting clearance results in smaller process forces, but higher stresses. The smallest von Mises stress occurs for 7° chamfer and 5 % cutting clearance, here however, the highest cutting forces occur in simulation and in experiment. To explain this phenomenon the contact area between punch and sheet was taken into account. Due to the higher bending moment for larger cutting clearances,

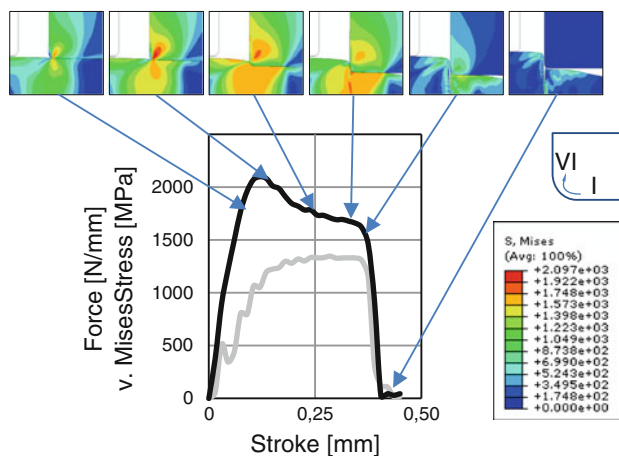


Fig. 8 Von Mises stress distribution in punch and maximum force and von Mises stress throughout cutting process (grey cutting force, black max. von Mises stress)

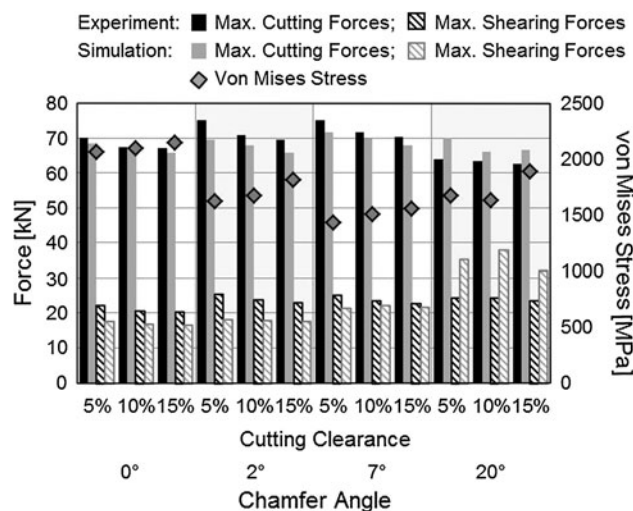


Fig. 9 Maximum cutting and shearing forces and maximum von Mises stresses in punch for all simulations and experiments

the sheet is bent away from the punch, which leads to a reduction of the contact area and therefore to higher stresses.

5 Conclusion

Within this research project, the possibilities for a reduction of the cutting and shearing forces during the shearing operation of PHS sheet materials as well as for the resulting stresses inside the punch were investigated. Therefore, an experimental shear cutting tool was introduced to determine the cutting and shearing forces and a FE-simulation model was presented to examine the stresses. Furthermore part quality was analyzed via profile measurements. The results of the determined force displacement curves

showed that the process parameters, cutting clearance and chamfer angle of the punch, have significant influences on the forces and stresses occurring during the cutting process. The application of a 20° chamfer angle led to a significant force reduction while stresses were fairly low, however parts could not reach sufficient quality. Using a 7° chamfer angle minimum stresses and sufficient part quality could be achieved, however very high forces occurred. In future work, the influence of the cutting process parameters on wear development and tool failure will be investigated.

Acknowledgments The research leading to these results has received funding from the European Union's Seventh Framework Programme (FP7/2007–2013) under grant agreement n° CP-FP 228841-2 (TailorTool).

References

- Goede M (2009) SuperLIGHT-car project—an integrated research approach for lightweight car body innovations. In: Proceedings of the international conference on innovative developments for lightweight vehicle structures, Germany, pp 25–38
- Banik J, Lenze FJ, Sikora S, Laurenz R (2011) Tailored properties—a pivotal question for hot forming. In: Proceedings of the 3rd international conference on hot sheet metal forming of high-performance steel, Germany, pp 13–20
- Mackensen A, Golle M, Golle R, Hoffmann H (2010) Experimental investigation of the cutting force reduction during the blanking operation of AHSS sheet materials. *CIRP Ann Manuf Technol* 59:283–286
- Fritz M (2011) Process optimization of laser cutting and in the heating process. In: Proceedings of the 3rd international conference on hot sheet metal forming of high-performance steel, Germany, pp 239–246
- Picas I, Hernández R, Casellas D, Valls I (2010) Strategies to increase the tool performance in punching operations of UHSS. In: Proceedings of the 50th IDDRG conference, Austria, pp 325–334
- Picas I, Muñoz R, Lara A, Hernández R, Casellas D (2011) Effect of the cutting process in the mechanical and fatigue properties of press hardened 22MnB5 steel. In: Proceedings of the 3rd international conference on hot sheet metal forming of high-performance steel, Germany, pp 85–92
- Hambli R, Reszka M (2002) Fracture criteria identification using an inverse technique method and blanking experiment. *Int J Mech Sci* 44:1349–1361
- So H, Faßmann D, Hoffmann H, Golle M, Schaper M (2012) An investigation of the blanking process of the quenchable boron alloyed steel 22MnB5 before and after hot stamping process. *J Mater Process Technol* 212:437–449
- Abaqus (2010) Abaqus 6.10 online documentation. Dassault Systèmes
- Bai Y, Wierzbicki T (2008) A new model of metal plasticity and fracture with pressure and Lode dependence. *Int J Plast* 24:1071–1096
- Beese A, Luo M, Li Y, Bai Y, Wierzbicki T (2010) Partially coupled anisotropic fracture model for sheets. *Eng Fract Mech* 77:1128–1152
- Bai Y, Wierzbicki T (2010) Application of extended Mohr–Coulomb criterion to ductile fracture. *Int J Fract* 161:1–20